DOI: 10.21062/mft.2025.058 © 2025 Manufacturing Technology. All rights reserved. http://www.journalmt.com

Geometric Accuracy of Elements Made Using the FFF Method from Selected Polymers with Different Internal Structure Densities

Malgorzata Gontarz-Kulisiewicz (0000-0002-1803-4415), Jacek Bernaczek (0000-0002-8942-092X), Mariusz Dębski (0000-0002-4889-7633)

Faculty of Mechanical Engineering and Aeronautics, Rzeszów University of Technology. Al. Powstańców Warszawy 12, 35-959 Rzeszów, Poland. E-mail: m.gontarz@prz.edu.pl, jacek.bernaczek@prz.edu.pl, m.debski@prz.edu.pl

Additive techniques are rapidly advancing due to their availability and ease of use, impacting both the industrial sector and individual users. The authors of numerous publications focus on the effects of specific printing parameters on the strength of models, usually made using selected MEX (Material Extrusion) methods. Among the MEX methods, the most frequently chosen are the FFF (Fused Filament Fabrication) and FDM (Fused Deposition Modeling) methods. This is due to the high accessibility and low cost of devices, as well as the wide availability of polymer materials. In their research, the authors increasingly consider the influence of the internal structure of the samples and their density on selected strength parameters, often without considering whether these factors influence the geometric accuracy of the sample being produced. Therefore, it was decided in the article to conduct research covering the indicated subject using the example of standardized samples made of six selected polymers used in the FFF method.

Keywords: MEX method, FFF method, Internal structure, Geometric accuracy, 3D printing

1 Introduction

Among the MEX methods, which use material extrusion to produce details, the most common is the FFF method [1]. This method is frequently used by researchers in the field of additive technologies due to several factors: the low costs of devices that support this technology, the high availability of polymer materials, and the high flexibility related to the individual setting of printing process parameters for defined applications and requirements resulting from the purpose of the produced model [2-4]. The compositions of polymer materials are increasingly modified to enhance their strength properties [5, 6].

Often in the aspect of scientific publications covering the FFF technology, there are studies covering the influence of selected process parameters on the strength of details, mainly made of a selected, single polymer material [7-10]. Rao et al. [11] in their studies analyzed the influence of the printing nozzle temperature on the tensile strength of samples made of PLA material with the addition of carbon fiber, considering various internal structures. Similarly, Tran et al. [12], after performing and describing the studies, found that increasing the temperature of the plasticizing nozzle during the production of models from ABS improved both the tensile and impact strength of the samples. Bhosale et al. [13] after analyzing the influence of the thickness of the print layer on the surface roughness, concluded that with its increase, the roughness also

increases. Similar conclusions were drawn by Baczkowski et al. [14]. Analyzing the studies available in the literature, it was found that layer thickness is a critical parameter of the printing process [15, 16]. Together with the orientation of the models relative to the working platform of the prototyping device [17], it significantly affects the strength of the produced components [18]. Additionally, in the studies related to the strength of elements made using the FFF method, the influence of the internal structure type, its density, and the direction of the fiber arrangement on various mechanical parameters in the bending test [19], compression [20, 21], tension [13, 22] and torsion [23] is often discussed. There are also studies that test the mechanical strength of recycled polymer materials [24]. However, there is a noticeable lack of studies regarding the accuracy of the detail reproduction using the FFF method, particularly in relation to the types of polymer materials used and the density of the selected internal structure [25, 26].

In connection with the above, an analysis was undertaken of the influence of selected polymer materials used in the FFF method of internal grid structure density on the geometric accuracy of reference samples - type 1A, used for the static tensile test, based on the PN-EN ISO 527-2:2012 standard [27, 28]. Six materials were selected for the tests, two commonly used pure materials: ABS (acrylonitrile-butadiene-styrene copolymer) and PLA (polylactide/polylactic

acid), two composite materials based on ABS, i.e. HABS (hard acrylonitrile-butadiene-styrene copolymer) and PC/ABS (polycarbonates), and two elastomeric materials: HIPS (high impact polystyrene) and an experimental composite of unknown composition: S&S (strong & soft) [29].

2 Experimental part

2.1 Samples for testing

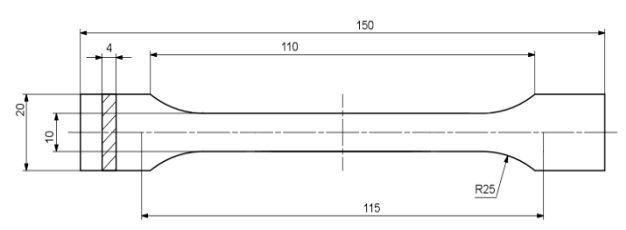


Fig. 1 Sample for strength test according to PN-EN ISO 527-2:2012 (dimensions given in [mm]) [28]

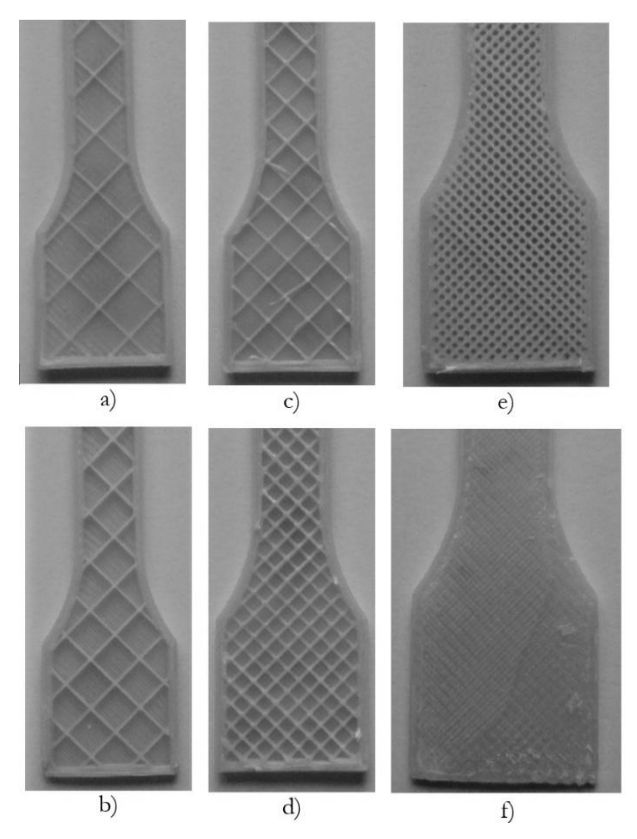


Fig. 2 The applied density of the internal grid-type structure on the example of samples made of PC/ABS material a) 13%; b) 15%; c) 20%; d) 65%; e) 80%; f) 100%

In the studies, the thickness and width of the narrow part of the standardized sample shapes used for the uniaxial tensile test were considered in the geometry analysis. Fig. 1 shows the applied dimensions of the sample that was tested. The sample was designed according to the PN EN ISO 527-2:2012 standard [27, 28] in a program for spatial modeling and the file

was exported to the .stl format. Fig. 2 illustrates the applied densities of the internal grid-type structure in the example of models made of PC/ABS.

2.2 Polymer materials used for research

The tested materials, their designations, the densities of the internal grid-type structure, as well as the temperatures of the plasticizing nozzle and the working platform, are given in Tab. 1.

Five samples were made for each density of the internal grid-type structure and each material (Tab. 1). The thickness of a single layer was set to 0.2 [mm]. It was assumed that five full layers would be made from the top and bottom of the sample. Samples made of ABS, HABS, PC/ABS, HIPS, and S&S materials were made using the UP BOX+ prototyping device with a closed thermal insulation chamber. Due to the device's perforated work table, a model support structure consisting of five layers was utilized. Due to the requirement for intensive cooling of samples made of PLA material after applying each layer, they were made on the Prusa i3 MK3 device (Prusa Research a.s, Prague, Czech Republic). The samples were positioned flat, and horizontally relative to the working platform of the prototyping devices. The arrangement of the samples in relation to the working platform of the device, taking into account individual axes and measured parameters, is presented in Fig. 3 in the software supporting the Prusa i3 MK3 device. Examples of the samples made are shown in Fig. 4.

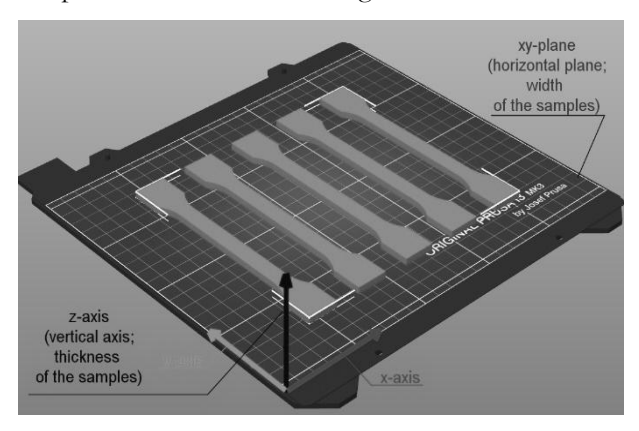


Fig. 3 Arrangement of samples relative to the working platform of the prototyping device

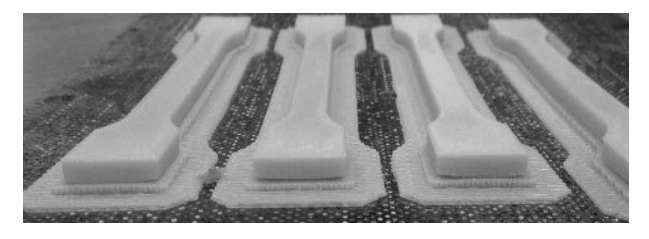


Fig. 4 Part of the view of sample samples made of PC/ABS material with an internal grid structure density of 13%

Tab. 1 Tested polymer materials [29]

Material	Symbol /	Temperature of the noz-	Temperature of the	
	Densities of the internal grid-type structure	zle [°C]	working platform [°C	
ABS	A13 / 13%	_		
	A15 / 15%		90	
	A20 / 20%	270		
	A65 / 65%			
	A80 / 80%	_		
	A100 / 100%			
	L13 / 13%	1	50	
	L15 / 15%	1		
PLA	L20 / 20%	210		
1 12/1	L65 / 65%			
	L80 / 80%	_		
	L100 / 100%			
	HA13 / 13%	_	100	
	HA15 / 15%			
HABS	HA20 / 20%	240		
11/103	HA65 / 65%	240		
	HA80 / 80%			
	HA100 / 100%			
	CA13 / 13%		100	
	CA15 / 15%			
PC/ABS	CA20 / 20%	260		
1 C/ MD3	CA65 / 65%	200		
	CA80 / 80%			
	CA100 / 100%			
	UH13 / 13%			
	UH15 / 15%		90	
HIPS	UH20 / 20%	235		
11113	UH65 / 65%	255		
	UH80 / 80%			
	UH100 / 100%			
S&S	S13 / 13%		<u> </u>	
	S15 / 15%		80	
	S20 / 20%	250		
	S65 / 65%	250		
	S80 / 80%]		
	S100 /100%	7		

3 Research methodology

After the tensile test specimens were made, the thickness and width of the narrow part of the specimens were measured using a Levenhuk DTX 90 digital microscope (Levenhuk Poland sp. z o. o., Warsaw, Poland). The width of the sample was measured at both ends and in the middle of the narrow part of the samples, while the thickness was measured three times in the middle of the element. This approach was necessary due to the shape of the samples and the limitations of the digital microscope's measuring area. The thickness of the narrow part of the specimen was measured relative to the Z direction (vertical axis) of the prototyping devices. The width of the narrow part of the specimen corresponds to the XY plane (horizontal plane) of the devices' worktable. An example of the thickness measurement for one sample is shown in Fig. 5.



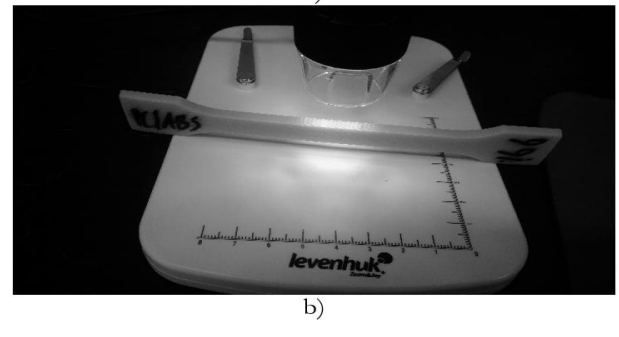


Fig. 5 Example of the thickness measurement for one sample

Before starting the geometry measurements of the samples, the microscope was calibrated for each analyzed height across all samples. After obtaining the results, the average value and standard deviation of the measured quantities for each sample were calculated, depending on the density of the internal structure and the polymer material. To verify and confirm the obtained results, several samples were also measured with a LogiLinkWZ0031 digital caliper (LogiLink (Tendberg GmbH), Schalksmühle, Germany).

Fig. 6 illustrates the sample thickness measurements of samples made of tested materials with internal structure density of grid type equal to 13%. Based on them, it was visually observed that the individual layer thicknesses varied depending on the orientation of the models relative to the worktable of the prototyping device. In samples made of HABS, HIPS, and

PC/ABS materials (Fig. 6c-e), it was visually determined that the thickness of individual layers is the same, except for the layer directly adjacent to the worktable (the bottom of the samples). A similar observation was made for samples made of S&S material, where the first three layers at the contact point with the work platform (Fig. 6f), are optically thicker than the others. For models made of ABS and PLA, it was visually observed that the layer thicknesses were the same (Fig. 6a-b). Similar properties were also visually noted in the other measured research samples with different applied internal structure densities.

Fig. 7 shows the measurement of the width of the narrow part of the sample. It was found that the edges of all samples were clear and sharp. The transparency of the samples made from S&S material (Fig. 7f) is related to the material properties.

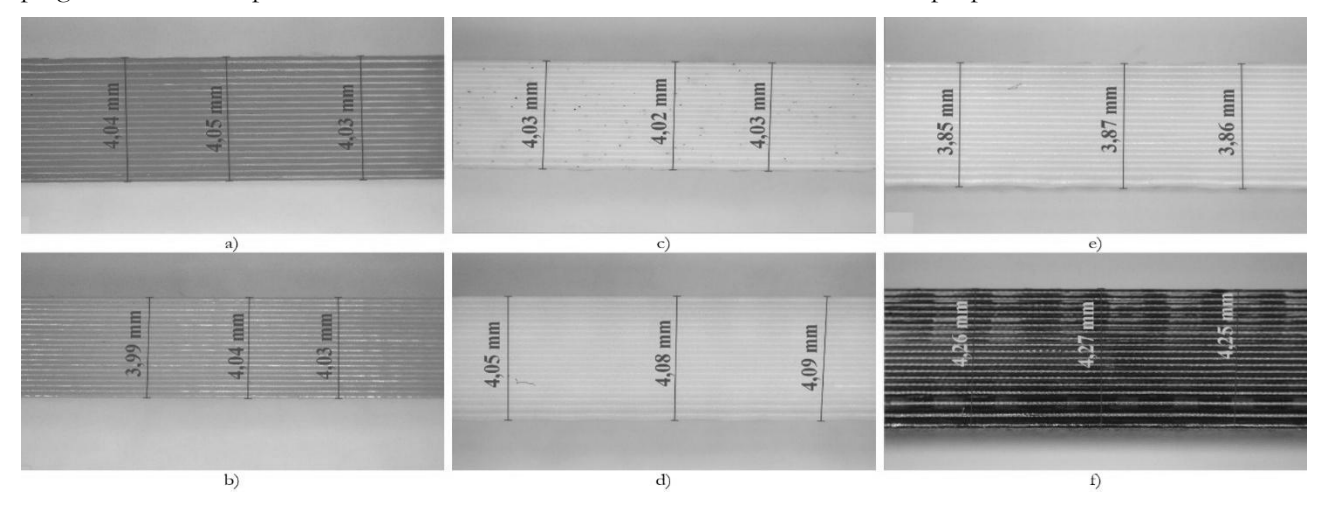


Fig. 6 Thickness measurement of samples with an internal structure density of 13% made of the tested polymer materials: a) ABS: 4.04/4.05/4.03; b) PLA: 3.99/4.04/4.03; c) HABS: 4.03/4.02/4.03; d) HIPS: 4.05/4.08/4.09; e) PC/ABS: 3.85/3.87/3.86; f) S&S: 4.26/4.27/4.25 (dimensions are given in [mm])

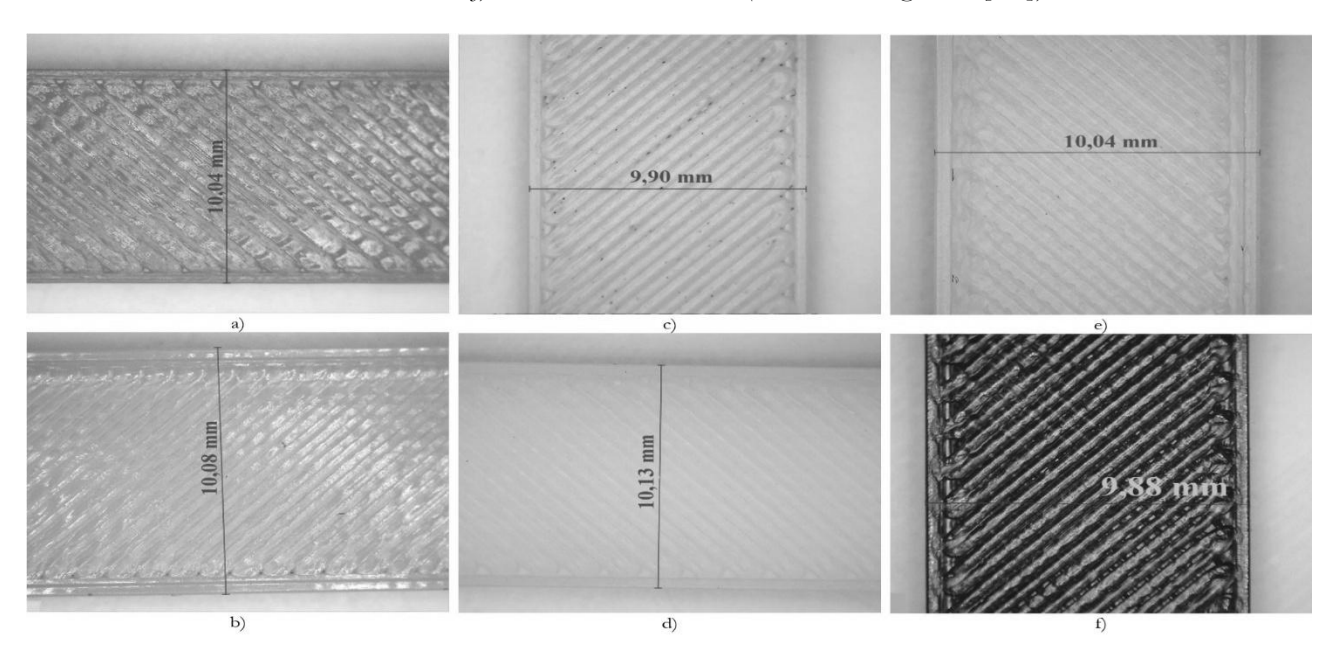


Fig. 7 Measurement of the width of the narrower part of sample samples with a nominal dimension of 10 [mm]: a) A13: 10.04; b) L13: 10.08; c) HA13: 9.90; d) UH13: 10.13; e) CA13: 10.04; f) S13: 9.88 (dimensions are given in [mm])

4 Development of measurement results

After the measurements were performed, summary tables were prepared to present the obtained results depending on the polymer material, the density of the internal structure, and the measured parameter. Below, in Tab. 2, the results examples of the measurement of the width of the narrow part of each of the

samples made of ABS material are included. In Tab. 3 and 4, there are average values of the measurements performed, respectively related to the width of the narrow part of the sample and to the thickness of the sample, together with the dimensional deviation determined by the nominal dimension for all the tested materials and the considered densities of the internal structure.

Tab. 2 Measurement results of the width of the narrow part of the ABS samples with a nominal size of 10 [mm]

Density of the internal	Sample number	Measurement results [mm]		Arithmetic	Standard deviation	Dimensio- nal devia-	
structure		No. 1	No. 2	No. 3	mean [mm]	[mm]	tion [mm]
13%	1	10.14	10.04	10.09	10.09	0.04	0.09
	2	10.05	10.03	10.03	10.04	0.01	0.04
	3	10.08	10.03	10.08	10.06	0.02	0.06
	4	10.20	10.18	10.19	10.19	0.01	0.19
	5	10.15	10.14	10.18	10.16	0.02	0.16
15%	1	10.16	10.15	10.14	10.15	0.01	0.15
	2	10.20	10.19	10.20	10.20	0.00	0.20
	3	10.13	10.12	10.14	10.13	0.01	0.13
	4	10.16	10.15	10.17	10.16	0.01	0.16
	5	10.16	10.15	10.11	10.14	0.02	0.14
20%	1	10.22	10.19	10.15	10.19	0.03	0.19
	2	10.17	10.16	10.17	10.17	0.00	0.17
	3	10.15	10.18	10.16	10.16	0.01	0.16
	4	10.19	10.16	10.18	10.18	0.01	0.18
	5	10.15	10.16	10.14	10.15	0.01	0.15
	1	10.15	10.12	10.16	10.14	0.02	0.14
	2	10.17	10.18	10.19	10.18	0.01	0.18
65%	3	10.15	10.13	10.14	10.14	0.01	0.14
	4	10.11	10.14	10.14	10.13	0.01	0.13
	5	10.20	10.19	10.20	10.20	0.00	0.20
80%	1	10.15	10.18	10.20	10.18	0.02	0.18
	2	10.17	10.14	10.16	10.16	0.01	0.16
	3	10.21	10.15	10.13	10.16	0.03	0.16
	4	10.17	10.21	10.15	10.18	0.02	0.18
	5	10.16	10.16	10.18	10.17	0.01	0.17
100%	1	10.18	10.15	10.16	10.16	0.01	0.16
	2	10.15	10.09	10.12	10.12	0.02	0.12
	3	10.15	10.12	10.16	10.14	0.02	0.14
	4	10.17	10.15	10.15	10.16	0.01	0.16
	5	10.15	10.17	10.19	10.17	0.02	0.17

Tab. 3 Measurement results of the width of the narrow part of samples with a nominal size of 10 [mm]

Material	Tested sample	Average value of the width measurement of the narrow part of the sample [mm]	Standard devia- tion [mm]	Dimensional devi- ation [mm]
ABS	A13	10.11	0.06	0.11
	A15	10.16	0.03	0.16
	A20	10.17	0.03	0.17
	A65	10.16	0.03	0.16
	A80	10.17	0.02	0.17
	A100	10.15	0.02	0.15
	L13	10.03	0.02	0.03
	L15	10.03	0.03	0.03
	L20	10.02	0.03	0.02
PLA	L65	10.04	0.02	0.04
	L80	10.06	0.02	0.06
	L100	10.02	0.03	0.02
	HA13	10.11	0.08	0.11
	HA15	10.14	0.02	0.14
	HA20	10.17	0.02	0.17
HABS	HA65	10.15	0.02	0.15
	HA80	10.16	0.01	0.16
	HA100	10.15	0.02	0.15
	CA13	10.05	0.02	0.05
	CA15	10.08	0.04	0.08
	CA20	10.09	0.03	0.09
PC/ABS	CA65	10.03	0.04	0.03
	CA80	10.03	0.02	0.03
	CA100	10.04	0.03	0.04
	UH13	10.19	0.03	0.19
	UH15	10.18	0.03	0.18
	UH20	10.17	0.07	0.17
HIPS	UH65	10.19	0.07	0.19
	UH80	10.18	0.02	0.18
	UH100	10.16	0.02	0.16
	S13	9.86	0.02	-0.14
S&S	S15	9.86	0.02	-0.14
	S20	9.85	0.01	-0.15
	S65	9.84	0.01	-0.16
	S80	9.86	0.02	-0.14
	S100	9.85	0.03	-0.15

Tab. 4 Results of thickness measurements of the narrow part of samples with nominal dimension 4 [mm]

Material	Tested sample	Average value of the thickness measurement of the narrow part of the sample [mm]	Standard deviation [mm]	Dimensional devi
ABS	A13	4.05	0.03	0.05
	A15	4.05	0.03	0.05
	A20	4.03	0.03	0.03
	A65	4.02	0.03	0.02
	A80	4.02	0.02	0.02
	A100	4.08	0.06	0.08
PLA	L13	3.99	0.03	-0.01
	L15	3.95	0.03	-0.05
	L20	3.98	0.04	-0.02
	L65	4.01	0.03	0.01
	L80	3.96	0.04	-0.04
	L100	4.01	0.02	0.01
HABS	HA13	4.03	0.02	0.03
	HA15	4.04	0.02	0.04
	HA20	4.07	0.02	0.07
	HA65	4.03	0.02	0.03
	HA80	4.05	0.03	0.05
	HA100	4.04	0.02	0.04
	CA13	3.89	0.05	-0.11
	CA15	3.94	0.07	-0.06
	CA20	4.15	0.08	0.15
PC/ABS	CA65	4.11	0.07	0.11
	CA80	4.06	0.09	0.06
	CA100	4.14	0.03	0.14
	UH13	4.06	0.03	0.06
	UH15	4.06	0.03	0.06
	UH20	4.06	0.03	0.06
HIPS	UH65	4.06	0.03	0.06
	UH80	4.06	0.02	0.06
	UH100	4.08	0.03	0.08
S&S	S13	4.27	0.02	0.27
	S15	4.30	0.06	0.30
	S20	4.23	0.06	0.23
	S65	4.31	0.05	0.31
	S80	4.18	0.16	0.18
	S100	4.28	0.12	0.28

To visualize the width and thickness measurement results presented in Tab. 3 and Tab. 4, the graphs in Fig. 8 and Fig. 9 were developed.

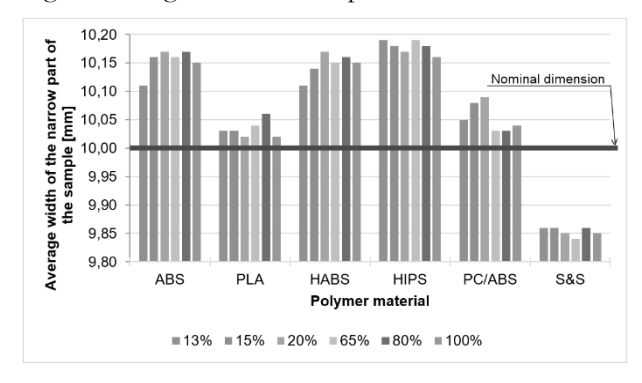


Fig. 8 Results of width measurements of samples made of tested polymer materials

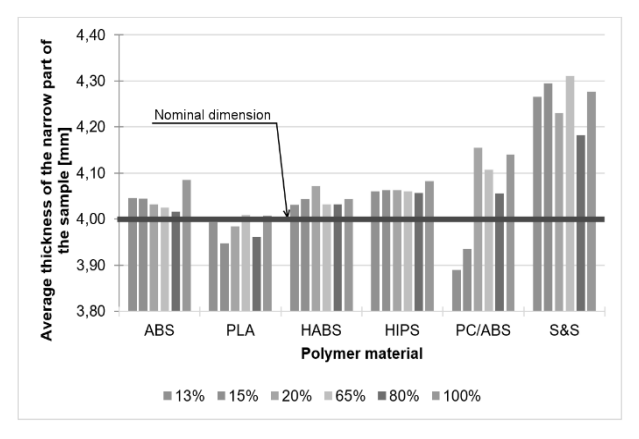


Fig. 9 The results of the thickness measurements of the narrow part of the samples made of six polymer materials

5 Discussion of measurement results

Samples made of HIPS and S&S materials are characterized by the lowest manufacturing accuracy in the horizontal plane (XY plane) (Tab. 3, Fig. 8). The average dimensional deviation for samples made from HIPS is 0.18 [mm], while for S&S samples, it is -0.15 [mm]. On the other hand, the average values of width measurements of samples made of PLA material are the closest to the nominal dimension (average value of dimensional deviation 0.03 [mm]) (Tab. 3, Fig. 8). This may be attributed to the fact that samples made of PLA material were made on the Prusa i3 MK3 device without a thermal insulation chamber due to the need for intensive cooling of individual sample layers. Among the samples manufactured on the UP BOX+ device, samples made of PC/ABS material are characterized by the smallest dimensional deviations (average value of dimensional deviation 0.05 [mm]) (Tab. 3, Fig. 8). Based on the data presented in Fig. 8, it was noted that for samples made of ABS and HABS materials, the inaccuracy of mapping also increases with the increase in the density of the internal structure. On the other hand, for samples made of PC/ABS with the density of the internal grid structure ranging from 65% to 100%, the dimensional deviation decreased by approx. 0.04 [mm] compared to samples with densities of 13% to 20% (Tab. 3, Fig. 8).

Comparing the results of the sample thickness measurements, measured about the vertical axis (Z axis) of the prototyping devices (Tab. 4, Fig. 9), it was found that the samples made of S&S material are characterized by the lowest geometric accuracy (average value of dimensional deviation 0.26 [mm]) compared to the other polymer samples. Similarly to the results of the sample width measurement, the accuracy of the PLA samples in terms of their thickness is also the highest (average value of dimensional deviation -0.02 [mm]). It is important to note that the results of the width measurements of the PLA samples were higher than the nominal dimension, in contrast to the results of their thickness measurement. The average value of the thickness measurement of the CA20-CA100 samples is higher than the nominal dimension (Fig. 9) by approx. 0.11 [mm] (Tab. 4).

According to the data presented in Fig. 9, the accuracy of manufacturing samples from HIPS material regarding the vertical axis of the prototyping device does not depend on the density of the internal structure. A similar pattern is observable in the measurements of HABS material, although samples made from HABS at a 20% internal structure density exhibit the highest dimensional deviation among the tested densities, measuring 0.07 [mm].

The accuracy of mapping elements made of ABS and HABS materials in the horizontal plane and in the vertical direction is comparable (Fig. 8-9). In the vertical axis, the average value of dimensional deviations was smaller (Fig. 9) than in the horizontal plane (Fig. 8). It was found that the geometric accuracy of the sample width (in the horizontal plane) for samples made of ABS and HABS materials does not depend on the density of the internal structure (Fig. 8). This independence is also observed for thickness measurements of HABS samples in the vertical direction (Fig. 9). On the other hand, for the thickness measurements of samples made of ABS, it was noted that accuracy improves with increasing density of the internal structure, excluding samples with full density (Fig. 9).

Samples made of HIPS material are characterized by greater inaccuracy in the mapping of the geometry of the narrow part of the sample in the XY plane (in the horizontal plane) (Fig. 8) compared to the accuracy of the production concerning the vertical axis (Fig. 9). It was also noted that the accuracy of the production of samples made of HIPS material is not affected by the density of the internal grid-type structure used.

The thicknesses of all measured samples made of S&S material exceed nominal dimension (Fig. 8), in contrast to the width measurements (Fig. 8).

This indicates that this S&S material is characterized by greater linear expansion in the vertical direction (average value of dimensional deviation 0.26 [mm]) (Tab. 4, Fig. 9) than in the horizontal direction (average value of dimensional deviation -0.15 [mm]) (Tab. 3, Fig. 8).

In summary, for both thickness and width measurements of the narrow part of the samples, the smallest dimensional deviations are found in models made of PLA material, whereas the largest deviations are found in S&S samples. However, considering the results of measurements of samples made on the UP BOX + prototyping device, the highest accuracy of reproduction was characteristic of samples made of PC/ABS material (Tab. 3-4, Fig. 8-9).

6 Conclusion

Based on the results of measurements of the geometry of the narrow part of the samples used in the tensile test, it was found that the density of the internal grid-type structure does not significantly affect the geometric accuracy of the samples.

Based on the obtained data, it was noted that for samples made of the following materials: ABS, PLA, HABS, and HIPS, the average dimensional deviation is smaller in the direction of the Z axis (vertical axis) compared to the horizontal plane (XY plane) of the prototyping device. In contrast, for samples made from S&S material, the reverse relationship was observed. Furthermore, the geometric accuracy of samples made of the PC/ABS material is comparable in both measured parameters. Based on the conducted tests, it was also found that the accuracy of sample reproduction depends on the properties of the polymer material and the accuracy of the prototyping device used.

To summarize the conducted research, it was concluded that the area of future work would be the verification of the potential influence of other available model filling patterns, such as linear, gyroidal, and honeycomb filling, on the geometric accuracy of models in the considered additive process. Additionally, as part of future research, it is planned to implement further processes for the final processing of models, which may also enhance geometric accuracy. The authors of the study also plan to produce reference research models taking into account the accuracy of manufacturing cylindrical, cuboid, and spherical elements, using other, alternative 3D printers using the FFF method, to conduct a comparative analysis of the results of measurements of geometric accuracy of models manufactured from identical model materials using different prototyping devices.

References

MANUFACTURING TECHNOLOGY

- [1] BULANDA, K., OLEKSY, M., OLIWA, R., BUDZIK, G., PRZESZŁOWSKI, Ł., FAL, J., JESIONOWSKI, T. (2021). Polymer Composites Based on Polycarbonate (PC) Applied to Additive Manufacturing Using Melted and Extruded Manufacturing (MEM) Technology. In: *Polymer*, Vol. 13. https://doi.org/10.3390/polym13152455
- [2] BUDZIK, G., MAGNISZEWSKI, M., PRZESZŁOWSKI, Ł., OLEKSY, M., OLIWA, J., BERNACZEK, J. (2018). Torsional strength testing of machine elements manufacture by incremental technology from polymeric materials (Rapid communication). In: Polimery, Vol. 63, No. 11-12, pp. 830-832. https://doi.org/10.14314/polimery.2018.11.13
- [3] DEBSKI, M., MAGNISZEWSKI, M., BERNACZEK, J., PRZESZŁOWSKI, Ł., GONTARZ, M., KIEŁBICKI, M. (2021). Influence of torsion on the structure of machine elements made of polymeric materials by 3D printing. In: *Polimery*, Vol. 66, No. 5, pp. 298-303. https://doi.org/10.14314/polimery.2021.5.3
- [4] SENKERIK, V., BEDNARIK, M., JANOSTIK, V., KARHANKOVA M., MIZERA, A. (2024). Analysis of Extrusion Process Parameters in PLA Filament Production for FFF Technology. In: *Manufacturing Technology*, Vol. 24, No. 2, pp. 265-271. DOI: 10.21062/mft.2024.037
- [5] KAYGUSUZ, B., ÖZERINÇ, S. (2019). Improving the ductility of polyactic acid parts produced by fused deposition modeling through polyhydroxyalkanoate additions. In: *Journal of Applied Polymer Science*, Vol. 136, Issue 43. https://doi.org/10.1002/app.48154
- [6] SINGH, P. K., MAUSAM, K., ISLAM, A. (2021). Achieving better results for increasing strength and life time of gears in industries using various composite materials. In: *Materials Today: Proceedings*, Vol. 45, pp. 3068-3074. https://doi.org/10.1016/j.matpr.2020.12.062
- [7] BUDZIK, G., DZIUBEK, T., PRZESZŁOWSKI Ł. P., SOBOLEWSKI, B., DĘBSKI, M., GONTARZ, M. E. (2023). Study of unidirectional torsion of samples with different internal structures manufactured in the MEX process. In: *Rapid Prototyping Journal*, Vol. 29, No. 8, pp. 1604-1619. https://doi.org/10.1108/RPJ-09-2022-0332

- [8] NAHAR, C., GURRALA, P. K. (2022). Transient thermal finite-element analysis of fused filament fabrication process. In: Rapid Prototyping Journal, Vol. 28, No. 6, pp. 1097-1110. https://doi.org/10.1108/RPJ-05-2021-0104
- [9] DEMIR, S., YÜKSEL, C. (2023). Evaluation of effect and optimizing of process parameters for fused deposition modeling parts on tensile properties via Taguchi method. In: *Rapid Prototyping Journal*, Vol. 29, No. 4, pp. 720-730. https://doi.org/10.1108/RPJ-06-2022-0201
- [10] ALEXOPOULOU, E., CHRISTODOULOU, I., T., MARKOPOULOS, A. P. (2024). Investigation of Printing Speed Impact on the Printing Accuracy of Fused Filament Fabrication (FFF) ABS Artefacts. In: Manufacturing Technology, Vol. 24, No. 3, 333-337. DOI: pp. 10.21062/mft.2024.042
- [11] RAO, V. D. P., RAJJV, P., GEETHIKA, N. (2019). Effect of fused deposition modeling (FDM) process parameters on tensile strength of carbon fibre PLA. In: *Materials Today: Proceedings*, Vol. 18, Part 6, pp. 2012-2018. https://doi.org/10.1016/j.matpr.2019.06.009
- [12] TRAN, T. Q., DENG, X., CANTURRI, C., THAM, C. L., NG, F. L. (2023). Highly-dense acrylonitrile butadiene styrene speciments fabricated by overheat material extrusion 3D printing, In: Rapid Prototyping Journal, Vol. 29, No. 4, pp. 687-696. https://doi.org/10.1108/RPJ-06-2022-0184
- [13] BHOSALE, V., GAIKWAD, P., DHERE, S., SUTAR, C., RAYKAR, S. J. (2022). Analysis of process parameters of 3D printing for surface finish, printing time and tensile strength. In: *Materials Today: Proceedings*, Vol. 59, Part 1, pp. 841-846. https://doi.org/10.1016/j.matpr.2022.01.210
- [14] BĄCZKOWSKI, M., MARCINIAK D., BIELIŃSKI, M. (2021). Influence of FFF process parameters and macrostructure homogenity on PLA impact strength (Rapid communication). In: *Polimery*, Vol. 66, No. 9, pp. 1-4. DOI: dx.doi.org/10.14314/polimery.2021.9.XXX
- [15] DEV, S., SRIVASTAVA, R. (2020). Experimental investigation and optimization of FDM process parameters for material and mechanical strength. In: *Materials Today: Proceeding*, Vol. 26, Part 20, pp. 1995-1999. https://doi.org/10.1016/j.matpr.2020.02.435

- [16] FONTANA, L., MINETOLA, P., IULIANO, L., RIFUGGIATO, S., KHANDPUR, M. S., STIUSO, V. (2022). An investigation of the influence of 3d printing parameters on the tensile strength of PLA material. In: *Materials Today: Proceedings*, Vol. 57, Part 2, pp. 657-663. https://doi.org/10.1016/j.matpr.2022.02.078
- [17] BECHNÝ, V., MATUŠ, M., JOCH, R., DRBÚL, M., CZÁN, A., ŠAJGALÍK, M., NOVÝ, F. (2024). Influence of the Orientation of Parts Produced by Additive Manufacturing on Mechanical Properties. In: *Manufacturing Technology*, Vol. 24, No. 1, pp. 2-8. DOI: 10.21062/mft.2024.021
- [18] DOSHI, M., MAHALE, A., SINGH, S. K., DESHMUKH, S. (2022). Printing parameters and materials affecting mechanical properties FDM-3D printed Parts: perspective and prospects. In: *Materials Today: Proceedings*, Vol. 50, Part 5, pp. 2269-2275. https://doi.org/10.1016/j.matpr.2021.10.003
- [19] BIROSZ, M. T., LEDENYÁK, D., ANDÓ, M. (2022). Effect of FDM infill patterns on mechanical properties. In: *Polymer Testing*, Vol. 113. https://doi.org/10.1016/j.polymertesting.2022.107654
- [20] PERNET, B., NAGEL, J. K., ZHANG, H. (2022). Compressive Strength Assessment of 3D Printing Infill Patterns. In: *Procedia CIRP*, Vol. 105, pp. 682-687. https://doi.org/10.1016/j.procir.2022.02.114
- [21] NACE, S. E., TIERNAN, J., HOLLAND, D., ANNAIDH, A.N. (2021). A comparative analysis of the compression characteristic of a thermoplastic polyurethane 3D printed in four infill patterns for comfort applications. In: *Rapid Prototyping Journal*, Vol. 27, No. 11, pp. 24-36. https://doi.org/10.1108/RPJ-07-2020-0155
- [22] NAIK, M., THAKUR, D. G., CHANDEL, S. (2022). An insight into the effect of printing orientation on tensile strength of multi-infill pattern 3D printed specimen: Experimental study. In: *Materials Today: Proceedings*, Vol. 62, Part 14, pp. 7391-7395. https://doi.org/10.1016/j.matpr.2022.02.305
- [23] BERNACZEK, J., DEBSKI, M., GONTARZ-KULISIEWICZ, M. (2024). Analysis of the Torsional Strength of Selected Photopolymers Additively Manufactured Using Polyjet Technology. In: *Manufacturing Technology*, Vol. 24, No. 6, pp. 865-870. DOI: 10.21062/mft.2024.094

- [24] PERNICA, J., VODÁK, M., ŠAROCKÝ, R., ŠUSTR, M., DOSTÁL, P., ČERNY, M., DOBROCKÝ, D. (2022). Mechanical Properties of Recycled Polymer Materials in Additive Manufacturing. In: *Manufacturing Technology*, Vol. 22, No. 2, pp. 200-203. DOI: 10.21062/mft.2022.017
- [25] JABBAR, M. A. (2023). A Design of Experiment Analysis Approach to Improve Part Quality in 3D Printing. In: *Manufacturing Technology*, Vol. 23, No. 3, pp. 290-297. DOI: 10.21062/mft.2023.034
- [26] FALES, A., ČERNOHLÁVEK, V., SUSZYNSKI, M., ŠTĚRBA, J., ZDRÁHAL,

- T., NOCAR, D. (2025). Experimental Measurement and Testing of 3D Printed Parts in Terms of the Material Used. In: *Manufacturing Technology*, Vol. 25, No. 2, pp. 174-184. DOI: 10.21062/mft.2025.016
- [27] PN-EN ISO 527-1:2020: Plastics-Determination of tensile properties-Part 1: General principles (https://sklep.pkn.pl/)
- [28] PN-EN ISO 527-2:2012: Plastics-Determination of tensile properties-Part 2: Test conditions for moulding and extrusion plastics (https://sklep.pkn.pl/)
- [29] https://f3dfilament.com/